Journal of Solid State Chemistry 184 (2011) 3336–3344

Contents lists available at SciVerse ScienceDirect

Journal of Solid State Chemistry

journal homepage: www.elsevier.com/locate/jssc

α- to β-$[C_6H_4(NH_3)_2]_2Bi_2I_{10}$ reversible solid-state transition, thermochromic and optical studies in the *p*-phenylenediamine-based iodobismuthate(III) material

Chakib Hrizi [a,*], Ameni Trigui [b], Younes Abid [b], Nassira Chniba-Boudjada [c], Pierre Bordet [c], Slaheddine Chaabouni [a]

[a] Laboratoire des Sciences de Matériaux et de l'Environnement (MESLab), Faculté des Sciences de Sfax (FSS), Université de Sfax, Route de Soukra km 3,5—BP 1171, 3018 Sfax, Tunisia
[b] Laboratoire de Physique Appliquée, Faculté des sciences de Sfax, Université de Sfax, BP 1171, 3018 Sfax, Tunisia
[c] Laboratoire de Cristallographie, CNRS, 25 avenue des Martyrs, BP 166, 3804 Grenoble Cedex 9, France

ARTICLE INFO

Article history:
Received 14 April 2011
Received in revised form
26 September 2011
Accepted 3 October 2011
Available online 20 October 2011

Keywords:
Organic–inorganic hybrid material
Iodobismuthates(III)
Phase transition
Thermochromism
Optical transmission
Photoluminescence

ABSTRACT

α-$[C_6H_4(NH_3)_2]_2Bi_2I_{10}$, which is a new material containing low-dimensional iodobismuthate anions, was synthesized and through its single crystal X-ray diffraction measurements, was proven to crystallize at room temperature in the centrosymmetric space group $P2_1/c$. It consists of a *p*-phenylenediammonium dication and a discrete (0-D) anion built up of edge-sharing bioctahedron. Due to the hydrogen bonds and the interatomic distances (Bi–I, I···I and π–π) changes, α-phase was transformed into the corresponding centrosymmetric β-phase, β-$[C_6H_4(NH_3)_2]_2Bi_2I_{10}$, through a single-crystal to single-crystal transformation occurring upon cooling to −28/−26 °C. Below the transition temperature, β-$[C_6H_4(NH_3)_2]_2Bi_2I_{10}$ crystallizes in the monoclinic system, centrosymmetric space group $P2_1/n$. Besides, the optical transmission measurements on α-$[C_6H_4(NH_3)_2]_2Bi_2I_{10}$ thin films have revealed two absorption bands at 2.47 and 3.01 eV. Finally, two room temperature photoluminescence emissions attributed to excitons radiative recombinations confined within the bioctahedra $Bi_2I_{10}^{4-}$, were observed in the red spectral range at 1.9 and 2.05 eV energy.

1. Introduction

In recent years, the interest in the magnetic, electronic and optoelectronic properties of low-dimensional organic–inorganic hybrid compounds [1–3] has increased, opening fascinating possibilities in several applications. Studies suggest that complex systems made up of organic and inorganic components have great potential for the creation of functional materials utilizing the wide variety of properties associated with each component [4,5]. In the fields of extensively studied halometalate hybrids, compounds based on Sn(II), Pb(II), Sb(III) and Bi(III) ions have shown to be of a great use in device applications due to their electronic [6–8] and optical properties [9–11]. Together with other related systems, the latter generally consist of zero- [12], one- [13,14] or two-dimensional [15] semiconductor networks of corners, edge-sharing or face-sharing divalent/or trivalent metal halide octahedra, separated by organic cations.

Owing to the low dimensionality of the inorganic semiconductor region, the stable excitons (electron–hole pair) have large binding energy of several hundred millielectron volts resulting from the quantum confinement effect and the enhanced dielectric confinement effect. Such properties allow strong excitonic absorption and emission even at room temperature [1,16]. Actually, the desired optical and electrical applications require simple and proper processing to obtain thin films with controllable thickness and uniformity.

It is thanks to the potentially semiconducting character of the inorganic frameworks [17,18] as well as the rich structural diversity displayed by these systems that bismuth iodide-based hybrids are interesting among the metal halides. The unique crystal chemistry of halobismuthate (III) is connected to the tendency of $[BiX_6]^{3-}$ octahedral to join each other through bridging halogen atoms, resulting in a large number of types of anionic sublattices characteristic of each stoichiometry. Concerning the observed differences in Bi–X bond lengths and X–Bi–X angles forming the mean values characteristic of non-deformed polyhedral, they were revealed to be linked to the shift of the lone electron pair (LEP) of the Bi(III) atom toward the interaction. As for the differences in Bi–X bond lengths, they are correlated to the primary deformations emanating from the tendency of

* Correspondence to: Sfax Faculty of Science, Chemistry Department, Soukra Road km 3,5—B.P. 1171, 3018 Sfax, Tunisia.
E-mail address: h_chakib1212@yahoo.fr (C. Hrizi).

0022-4596/$ - see front matter © 2011 Elsevier Inc. All rights reserved.
doi:10.1016/j.jssc.2011.10.004

octahedrons $[BiX_6]^{3-}$ to share halogen atoms and secondary deformations generated from intermolecular interactions. N–H···X hydrogen bonds also distort octahedrons $[BiX_6]^{3-}$, shifting the halogen atoms in the direction of the positively charged cations [19].

The present paper reports on the synthesis, structural transformation of the high and low temperature phases as well as the reversible phase transition characterized by differential scanning calorimetry (DSC). It also accounts for the optical properties of a new iodobismuthate-based hybrid compound, α-$[C_6H_4(NH_3)_2]_2Bi_2I_{10}$.

2. Experimental details

2.1. Synthesis

The α-$[C_6H_4(NH_3)_2]_2Bi_2I_{10}$ crystal was prepared by dissolving $Bi(NO_3)_3$ (0.5 g, 1.265 mmol, 99%) and *p*-phenylenediamine (0.139 g, 1.227 mmol, 97%) in concentrated HI solution (57 wt%, $d=1.70$) in stoichiometric reaction. It is worthwhile to mention that such reaction occurred in the presence of ethanol (50 ml). After being heated to 90 °C for 30 min, the solution was filtered and allowed to evaporate at room temperature till the formation of dark red prismatic monocrystals in the solution. The elemental analysis of the obtained crystals was performed in a dispersive energy spectrometer and yielded: Bi—21, 91; I—66, 53; C—7, 55 and N—2, 93%. Calculated for α-$[C_6H_4(NH_3)_2]_2Bi_2I_{10}$: Bi—21, 57; I—65, 62; C—7, 61 and N—2,82%.

2.2. Crystal structure determination

The data pertaining to the compound α-$[C_6H_4(NH_3)_2]_2Bi_2I_{10}$ at 20 °C were collected using a Bruker APEXII CCD four-circle diffractometer with graphite-monochromated (Mo*K*α). Besides, a suitable crystal of the *β*-$[C_6H_4(NH_3)_2]_2Bi_2I_{10}$ at –123 °C was glued to a glass fiber mounted on a Nonius Kappa CCD four-circle diffractometer with graphite-monochromated (Mo*K*α). Next, an empirical absorption correction based on symmetry equivalent reflections was applied using the SADABS [20] program. It is to be noted that pertinent details of the crystal structures of $[C_6H_4(NH_3)_2]_2Bi_2I_{10}$ at 20 and −123 °C are presented in Table 1 and a complete list of the atomic coordinates as well as the

Table 1
Crystal data and structure refinement details for α- and *β*-$[C_6H_4(NH_3)_2]_2Bi_2I_{10}$ at 20 and −123 °C.

Compound	α-$[C_6H_4(NH_3)_2]_2Bi_2I_{10}$	*β*-$[C_6H_4(NH_3)_2]_2Bi_2I_{10}$
Crystal data		
Empirical formula	$C_6H_{10}N_2BiI_5$	$C_6H_{10}N_2BiI_5$
Formula weight (g/mol)	953.66	953.66
Crystal system	Monoclinic	Monoclinic
Space group	$P2_1/c$	$P2_1/n$
a (Å)	12.053(5)	11.4827(3)
b (Å)	12.846(7)	12.9016(3)
c (Å)	12.506(6)	14.9698(4)
β (Å)	117.46(5)°	112.40(5)°
v (Å^3)	1718.2(16)	2050.37(9)
Z	4	4
D_{calc} (g cm^{-3})	3.686	3.089
Absorption coefficient	19.221	16.107
μ (mm^{-1})	19.22	16.11
F(000)	1632	1632
Crystal size (mm)	0.26 × 0.17 × 0.08	0.23 × 0.15 × 0.08
Crystal habit	Dark-red prism	Orange prism
Data collection		
Diffractometer	Bruker APEXII CCD Diffractometer	Nonius Kappa CCD Diffractometer
Monochromator	Graphite	Graphite
Radiation type, *λ* (Å)	Mo*K*α, 0.71073 Å	Mo*K*α, 0.71073 Å
T (K)	293(2)	150(2)
Θ range (deg.)	3.6–27.5	1.9–29.5
Indexes range	$-14 \le h \le 14$ $-15 \le k \le 16$ $-16 \le l \le 14$	$-15 \le h \le 14$ $-17 \le k \le 16$ $-18 \le l \le 20$
Absorption correction	Multi-scan (SADABS)	Multi-scan (SADABS)
T_{min}/T_{max}	0.0381/0.2149	0.060/0.241
Measured reflections	9427	13831
Independent reflections	3144	5708
Observed refl. ($I > 2\sigma(I)$)	1761	1664
R_{int}	0.048	0.052
Refinement		
Refinement on	F^2	F^2
Data/restraints/parameters	1761/0/127	1664/0/127
$R(F_0^2) > 2\sigma(F_0^2)$	$R_1=0.0562$ w$R_2=0.1224$	$R_1=0.0442$ w$R_2=0.1160$
R (all data)	$R_1=0.0562$ w$R_2=0.1224$	$R_1=0.0442$ w$R_2=0.1160$
GooF=*S*	0.8751	0.9581
$\Delta\rho_{max}/\Delta\rho_{min}$ (e Å^{-3})	2.67 (1.08 Å from Bi1)/ −2.13 (0.97 Å from Bi1)	4.52 (0.90 Å from Bi1)/ −1.16 (0.84 Å from Bi1)
CCDC deposit number	811,056	811,057

anisotropic motion parameters for each compound is given as "Supporting Information".

Both structures were solved in the monoclinic symmetry, in the centrosymmetric space groups $P2_1/c$ at 20 °C and $P2_1/n$ at −123 °C. Regarding bismuth and iodine atoms, they were located using the Patterson methods with SHELX-86 program [21]. As for the carbon and nitrogen atoms, they were brought about from successive difference Fourier calculations using CRYSTALS [22] computer program. The structures were refined by full-matrix least-squares using anisotropic temperature factors for all non-hydrogen atoms. Although H atoms were all located in a difference maps, those attached to carbon atoms were repositioned geometrically. The former were geometrically fixed at the calculated positions attached to their parent atoms, and treated as riding atoms.

2.3. Physicochemical characterization techniques

IR spectra were recorded in the range 400–4000 cm^{-1} (see Fig. S2, Supporting Information) using a Nicolet Impact 410 spectrometer by transmission through KBr pellets containing 1% of the crystals. The differential scanning calorimetry analysis was performed with a DSC 822P METTLER TOLEDO instrument for temperatures ranging from −100 to 30 °C at a rate of 5 and 10 °C min^{-1} upon cooling and heating. A polycrystalline sample of 7 mg was placed in a hermetic aluminum cell into a nitrogen atmosphere. Thermogravimetric analysis (TGA) experiments were performed from room temperature to 250 °C using a ATG PYRIS 6 instrument analyzer under nitrogen at a heating rate 5 °C min^{-1} (see Fig. S3, Supporting Information). Powder X-ray diffraction patterns were recorded using a D8 Bruker diffractometer (Cu$K\alpha_1$ 1.5406 Å) equipped with a front monochromator. The photoluminescence spectrum was recorded at room temperature by means of the 488 nm line of the argon ion LASER and an HORIBA JOKIN-YVON (HR320) spectrometer. In order to avoid the sample heating, the laser power is limited to 10 mW. Thin films of α-$[C_6H_4(NH_3)_2]_2Bi_2I_{10}$, whose optical absorption spectra were measured at room temperature using a UV–vis absorption spectrometer (Hitachi, U-3300), were formed on a quartz substrate by spin coating at 800 rpm and for 45 s duration.

3. Results and discussion

3.1. Structure description

The single crystal X-ray analysis showed that α-$[C_6H_4(NH_3)_2]_2Bi_2I_{10}$ compound crystallized at room temperature in the space group $P2_1/c$. Its structure can be easily described relating to $[C_6H_4(NH_3)_2]_2Bi_2I_{10}\cdot 4H_2O$ [23]. The asymmetric unit of the title compound comprised one *p*-phenylenediammonium dication and one-half of a dimeric decaiododibismuthate tetraanion. In fact, the latter generated the tetraanion from an inversion center, via $Bi-I1-Bi^{i}$ and $Bi-I1^{i}-Bi^{i}$ bridges $[-x+1, -y, -z+2]$ to build the complex $(C_6H_4(NH_3)_2^{2+})_2(Bi_2I_{10}^{4-})$. An overview of the formula unit made up of two cations and one anion is shown in Fig. 1. The $(Bi_2I_{10})^{4-}$ anionic species has been frequently observed in bismuth halide chemistry [24,25]. In our context, and as expected, the $Bi–I_{terminal}$ bond lengths (mean value of 3.0091 Å) were displayed as significantly shorter than the $Bi–I_{bridging}$ bond lengths (mean value of 3.2792 Å) (see Table 2). The deviations from regular octahedra also concerned the I–Bi–I bond angles with $I_{terminal}–Bi–I_{terminal}$ angles greater than 90° (mean value of 91.17°) and $I_{bridging}–Bi–I_{bridging}$ angles smaller than 90° (86.81°). This distortion in the angles could be interpreted as the beginning of localization of the lone pairs trans to the Bi–Bi vector, and/or a geometric arrangement to minimize the Bi–Bi interaction [12-a].

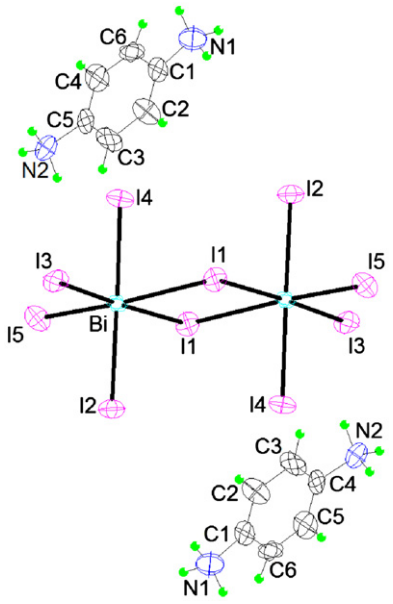

Fig. 1. The asymmetric unit of the α-$[C_6H_4(NH_3)_2]_2Bi_2I_{10}$ compound showing the atom numbering scheme.

Fig. 2 shows views of the crystal packing in α-$[C_6H_4(NH_3)_2]_2Bi_2I_{10}$. In fact, stacked in a chessboard fashion, inorganic–organic hybrid layers were observed for the compound. The inorganic sheets of $Bi_2I_{10}^{4-}$ anions were inserted between the organic layers in α-$[C_6H_4(NH_3)_2]_2Bi_2I_{10}$. In the same sheet, the binuclear anions were close enough in space to participate in $I\cdots I$ interactions between the anions ($I(5)\cdots I(5)' = 4.069(7)$ Å, $I(2)\cdots I(3)' = 4.367(4)$ Å), and connect them into pseudo-two-dimensional layers. Each of the ammonium parts of molecules points to the holes of the inorganic sheet and are linked to the iodine atoms (d(N–H···I) in the range 3.413–3.844 Å) of both $Bi_2I_{10}^{4-}$ anions in neighboring layers, bringing the anions together (Fig. 2). Close interactions between iodides on adjacent sheets including ($I(1)\cdots I(4)' = 3.893(3)$, $I(2)\cdots I(5)' = 4.069(3)$ and $I(3)\cdots I(5)' = 4.228(2)$ Å) served to tether the anions in adjacent sheets together into a pseudo-three-dimensional array (which extended along the *c* axis of the structure). These distances were slightly less than twice the ionic radius for the iodide ion (2.2 Å) [26], indicating that the binuclear anions were in close contact within the inorganic layers.

α-$[C_6H_4(NH_3)_2]_2Bi_2I_{10}$ compound exhibited a phase transition at −28/−26 °C, which was first characterized from DSC analysis. The unit-cell of the low temperature β-phase was confirmed by single-crystal X-ray analysis. Next, the unit-cell transformation from α- to β-phases resulted in a change of parameters in the $a-c$ plan. The volume of the β-phase is ~1.2 as big as the α-phase one. The *c*-glide plane changes only its designation to *n*, due to the changed *a* and *c* axes directions. This behavior is similar to that observed in the compound $[C_3H_5N_2]_3[Sb_2Br_9]$ [27]. Then, the structure of β-$[C_6H_4(NH_3)_2]_2Bi_2I_{10}$ is described in the space group $P2_1/n$. Indeed, the asymmetric unit is constituted by half of the dimeric decaiododibismuthate tetraanions having the geometry of two octahedra sharing one edge and one *p*-phenylenediammonium dication. β-$[C_6H_4(NH_3)_2]_2Bi_2I_{10}$ differs from $[C_6H_4(NH_3)_2]_2Bi_2I_{10}\cdot 4H_2O$ [23] only by the absence of a water molecules of crystallization in formulation unit. The shape and environment of the dimeric decaiododibismuthate tetraanion are approximately the same as the bioctahedron anion in $[C_6H_4(NH_3)_2]_2Bi_2I_{10}\cdot 4H_2O$. Fig. 3 shows the zero-dimensional (0D) periodic arrangement of the edge sharing Bi_2I_{10} bioctahedra and the organic $H_3N(C_6H_4)NH_3$ dications. The Bi

Table 2
Crystal data and structure refinement details for α- and β-$[C_6H_4(NH_3)_2]_2Bi_2I_{10}$ at 20 and −123 °C.

Parameters	20 °C	−123 °C	Change
Bond length (Å)			
Bi–I1	3.182 (2)	3.271 (2)	+0.089(2)
Bi–I2	3.066 (2)	3.101 (2)	+0.035(2)
Bi–I3	3.005 (2)	2.923 (2)	−0.082(2)
Bi–I4	3.069 (2)	3.064 (2)	−0.005(2)
Bi–I5	2.895 (3)	2.951 (2)	+0.056(3)
Bi–$I1^i$	3.382 (3)	3.246 (2)	−0.136(3)
C1–C2	1.33 (3)	1.35 (4)	+0.02(4)
C3–C2	1.43 (4)	1.40 (4)	−0.03(4)
C4–C3	1.35 (4)	1.34 (4)	−0.01(4)
C5–C4	1.38 (4)	1.33 (4)	−0.05(4)
C5–C6	1.34 (4)	1.31 (4)	−0.03(4)
C6–C1	1.40 (4)	1.35 (4)	−0.05(4)
N1–C1	1.45 (3)	1.44 (3)	−0.01(3)
N2–C4	1.46 (3)	1.46 (3)	0.00
Bi···Bi distances			
$Bi1\cdots Bi1^i$	4.770(5)	4.563(2)	−0.207
Bond angles (deg.)			
$I1^i$–Bi–I3	89.31 (9)	90.25(7)	
$I1^i$–Bi–I2	95.55 (9)	91.46(6)	
I3–Bi–I2	88.68 (8)	89.18(7)	
$I1^i$–Bi–I4	86.22 (8)	87.38(5)	
I3–Bi–I4	91.92 (8)	91.54(7)	
I2–Bi–I4	178.14 (6)	178.64(7)	
$I1^i$–Bi–I1	86.81 (8)	91.13(5)	
I3–Bi–I1	175.98 (6)	177.36(7)	
I2–Bi–I1	92.76 (8)	88.54(6)	
I4–Bi–I1	86.75 (8)	90.77(6)	
$I1^i$–Bi–I5	173.93 (6)	177.84(7)	
I3–Bi–I5	94.89 (9)	89.86(8)	
I2–Bi–I5	88.93 (9)	90.70(7)	
I4–Bi–I5	89.27 (9)	90.46(6)	
I1–Bi–I5	88.89 (9)	88.85(7)	
Bi–I1–Bi^i	93.19 (8)	88.87(5)	
C6–C5–C4	117 (2)	118(3)	
C5–C6–C1	122 (3)	124(3)	
N2–C4–C5	119 (2)	120(3)	
N2–C4–C3	118 (2)	119(3)	
C5–C4–C3	123 (2)	121(3)	
N1–C1–C6	119 (2)	125(3)	
N1–C1–C2	121 (3)	117(3)	
C6–C1–C2	120 (2)	119(3)	
C4–C3–C2	118 (2)	121(3)	
C3–C2–C1	120 (2)	117(3)	

Symmetry code: (i) $-x+1, -y, -z+2$ (at 20 °C); $-x+1, -y+1, -z+1$ (at −123 °C).

coordination environment of the dimeric $[Bi_2I_{10}]^{4-}$ tetraanions had the geometry of a substantially distorted octahedron, with the *cis* and *trans* angles in the ranges 89.91(3)–91.12(2)° and 177.20(2)–178.57(2)°, respectively. The bond lengths between the bismuth atoms and terminal iodine varied between 2.923(2) and 3.101(2) Å, while the distances to the two bridging iodine atoms were considerably longer, 3.246(2)–3.271(2) Å. As previously mentioned, the LEP is responsible for the deformation of the octahedron coordination sphere of Bi(III). There was a shift of the lone electron pair in the direction of the bridging iodine atom and resulting charge depletion at the opposite Bi−I bond.

For β-$[C_6H_4(NH_3)_2]_2Bi_2I_{10}$, the inorganic sheets of $Bi_2I_{10}^{4-}$ anions were sandwiched between the organic layers of $C_6H_4(NH_3)_2^{2+}$. In the inorganic sheet, closer I···I interactions of 3.718 Å between iodides on adjacent Bi_2I_{10} bioctahedrons within a layer including $I(3)\cdots I(5)'$ were proven. These quite short values, slightly shorter than twice the ionic radius of the iodide ion (2.2 Å) [26], linked the anionic components within a sheet in pseudo-two-dimensional layers running along the [0 1 0] crystallographic direction (see Fig. 3). Other close interactions between iodides on adjacent layers including $(I(3)\cdots I(4)' = 4.204$ Å) assured the cohesion of the crystalline building, giving rise to a pseudo-three-dimensional (3-D) construction of the structure and adding stability to this compound.

The two dimers in the α- and the β-phases were significantly different in the metal iodide bond distances. The iodine bridge involving Bi in the α-$[C_6H_4(NH_3)_2]_2Bi_2I_{10}$, in which the $Bi–I(1)_{bridge}$ bond distance was about 0.2 Å shorter than $Bi–I(1)^i_{bridge}$, which in turn was associated with an angle $Bi1-I1-Bi1^i$ of 86.81(8)°, was rather asymmetric (see Table 2). Yet, the dimer in the second phase β-$[C_6H_4(NH_3)_2]_2Bi_2I_{10}$ was symmetric with the two Bi–I bond distances equal to (3.246(2)–3.271(2)Å) with values between those of the Bi–I bond distances of the asymmetric bridge.

The most significant changes occurred in the reduction of the intra-ionic Bi/Bi distances on lowering the temperature (see Table 2); however, the intra-ionic distance of the α-phase is longer than 4.68 Å, while in the β-phase is shorter than 4.68 Å, a value, which corresponds to twice the van der Waals radius of bismuth [28].

It is worthwhile to mention that in the two phases (α and β), the role of H bond interactions with the surrounding cations was important for the anion geometries. In fact, in the α-$[C_6H_4(NH_3)_2]_2Bi_2I_{10}$ (asymmetric dimer), the hydrogen atoms of the ammonium groups (H13–N1, H23–N2 and H22–N2) of the *p*-phenylenediammonium dications were involved in bifurcated hydrogen bond interactions with ($I2^{ii}$ and $I1^{ii}$), ($I5^{Ivi}$ and $I2^{Ivi}$) and ($I4^{vi}$ and $I3^{vi}$), respectively. Besides, the (H11–N1 and H21–N2 hydrogen atoms) interacted again with I1 and $I3^{iii}$. In the β-$[C_6H_4(NH_3)_2]_2Bi_2I_{10}$ (symmetric dimer), the iodides ($I4^{vIIi}$ and $I4^{vIIIi}$) were involved in hydrogen bond interactions with (H21–N2 and H11–N1) while $I2^{vIi}$ had an interaction with (H21–N2). The bridging iodide I1 and $I1^i$ were not linked by hydrogen bond interactions. Details of the hydrogen bonding interactions present in both α- and β-$[C_6H_4(NH_3)_2]_2Bi_2I_{10}$ are listed in Table 3.

A view along the long molecular axis of the organic layer of the α- and β-$[C_6H_4(NH_3)_2]_2Bi_2I_{10}$ phases is given in Fig. 4. Indeed, in β-$[C_6H_4(NH_3)_2]_2Bi_2I_{10}$, the crystal packing reported in Fig. 4b shows the parallel orientation of the *p*-phenylenediammonium dications with intermolecular distances of about 5 Å characteristic of weak π interactions among the molecules, leading to a regular molecular packing. The description of the packing of the α-$[C_6H_4(NH_3)_2]_2Bi_2I_{10}$ was deduced from the β-phase by considering, from a geometric point of view, a rotation of the molecules at $y=1/2$ by approximately 90° along their long molecular axis (Fig. 4a). The molecular packing was determined by the previously discussed hydrogen bond interactions and the strong π interactions of the *p*-phenylenediammonium dications with the intermolecular distances between the relative molecular planes ranging from 3.5 to 3.8 Å, which strongly contributed to the crystal packing.

The main geometrical features of $[C_6H_4(NH_3)_2]^{2+}$ entities are reported in Table 2. The interatomic bond lengths and angles were similar in the two molecules of the α- and β-$[C_6H_4(NH_3)_2]_2Bi_2I_{10}$. The organic molecular ring in α-$[C_6H_4(NH_3)_2]_2Bi_2I_{10}$ built up by (C1, C2, C3, C4, C5 and C6) was less planar than that in the β-$[C_6H_4(NH_3)_2]_2Bi_2I_{10}$ (rms deviations of fitted atoms equal to 0.0152 and 0.0149).

3.2. X-ray powder diffraction

The X-ray powder diffraction pattern (Fig. S1, Supporting Information) of selected ground crystals has been fully indexed starting from the unit cell parameters obtained from single crystal data. The parameters have been refined using the Fullprof program giving $a=11.6650(3)$ Å, $b=12.1282(7)$ Å, $c=12.1077(5)$ Å, $\beta=117.34(6)°$ and $V=1521.635(7)$ Å^3 in agreement with the data of Table 1.

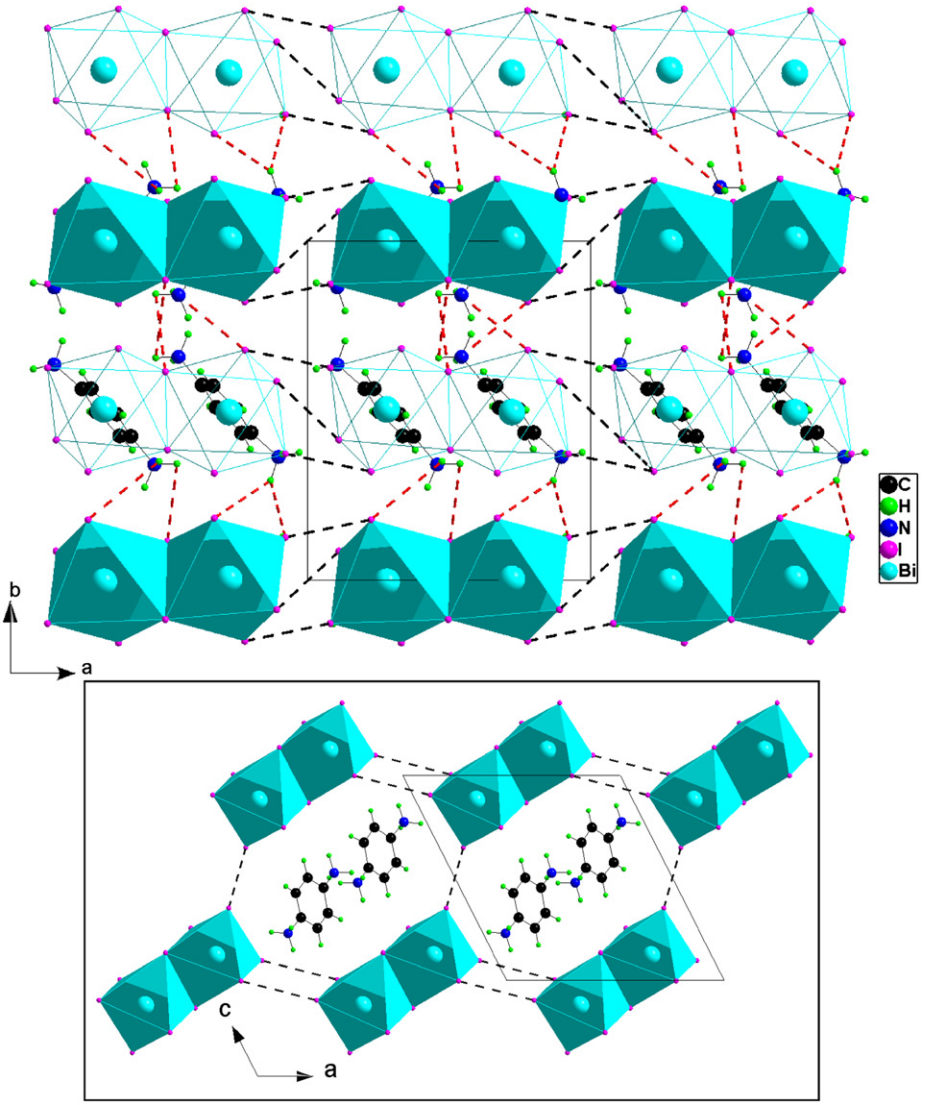

Fig. 2. View of the structure of α-$[C_6H_4(NH_3)_2]_2Bi_2I_{10}$ along the *c* axis showing the cation–anion alternating layers with I···I interactions and N–H···I hydrogen bonds (dashed lines), (insert shows a chessboard fashion viewed along the *a*-axis (dashed lines indicate electrostatic interactions within a sheet)).

Complete analysis of the powder pattern confirms that α-$[C_6H_4(NH_3)_2]_2Bi_2I_{10}$ crystallizes in the monoclinic $P2_1/c$ system. The density was measured at room temperature by flotation in tetrachlorobenzene. The average value of density, $D_m = 3.43\ g\ cm^{-3}$, yields a value of four formula units and a calculated density, $D_{calc} = 3.68\ g\ cm^{-3}$.

3.3. Infrared spectroscopy

The IR spectrum of α-$[C_6H_4(NH_3)_2]_2Bi_2I_{10}$ (given as Supporting Information) shows at high wavenumbers an absorption centered at 3026 cm^{-1} assignable to $\nu(NH_3^+)$. The bands at 2830, 2532 and 2423 cm^{-1} were associated with the ν(C–H) of the aromatic ring. The bands observed at 1767, 1620 cm^{-1} are attributed to δ(NH). The bands at 1499, 1385 and 1317 cm^{-1} are assigned to stretching vibrations of C=C, which also can be observed in the IR of the compound $[C_6H_4(NH_3)_2]_2Bi_2I_{10}\cdot 4H_2O$ [23]. The band at 1262 cm^{-1} is associated with the ν(C–N) and ν(C=C) of the aromatic ring. The vibrations at 1163 and 1114 cm^{-1} are due to the deformation of C-C-H bands (δ(CCH)) and that at 1025, 1001 and 826 cm^{-1} to γ(CCH) of the phenyl group, while the bands in the 747–434 cm^{-1} range may be assigned to γ(CCC) and δ(CCC) of the *p*-phenylenediammonium.

The spectra of the present compound and the $[C_6H_4(NH_3)_2]_2Bi_2I_{10}\cdot 4H_2O$ [23] are different in the absorption bands associated to the water molecules. The strong and broad absorption band with the major peak at 3450 cm^{-1} and the strong peak at 1585 cm^{-1} (in the $[C_6H_4(NH_3)_2]_2Bi_2I_{10}\cdot 4H_2O$ compound) assigned to $\nu(H_2O)$ and $\delta(H_2O)$, respectively, are not present in the IR spectrum of the α-$[C_6H_4(NH_3)_2]_2Bi_2I_{10}$.

3.4. Differential scanning calorimetry

The DSC curves obtained for α-$[C_6H_4(NH_3)_2]_2Bi_2I_{10}$ crystals upon cooling and heating scans are illustrated in Fig. 5. Several scans were carried out below room temperature. The first anomaly upon cooling appears at −31 °C (5 °C/min, scan 1), whereas on heating (5 °C/min, scan 2) it takes place at −26 °C. Next cooling (10 °C/min, scan 3) reveals the anomaly at −28 °C and upon second heating it is reversible at −26 °C. From the calorimetric measurements one can conclude that the title compound discloses one discontinuous reversible phase transition of first-order

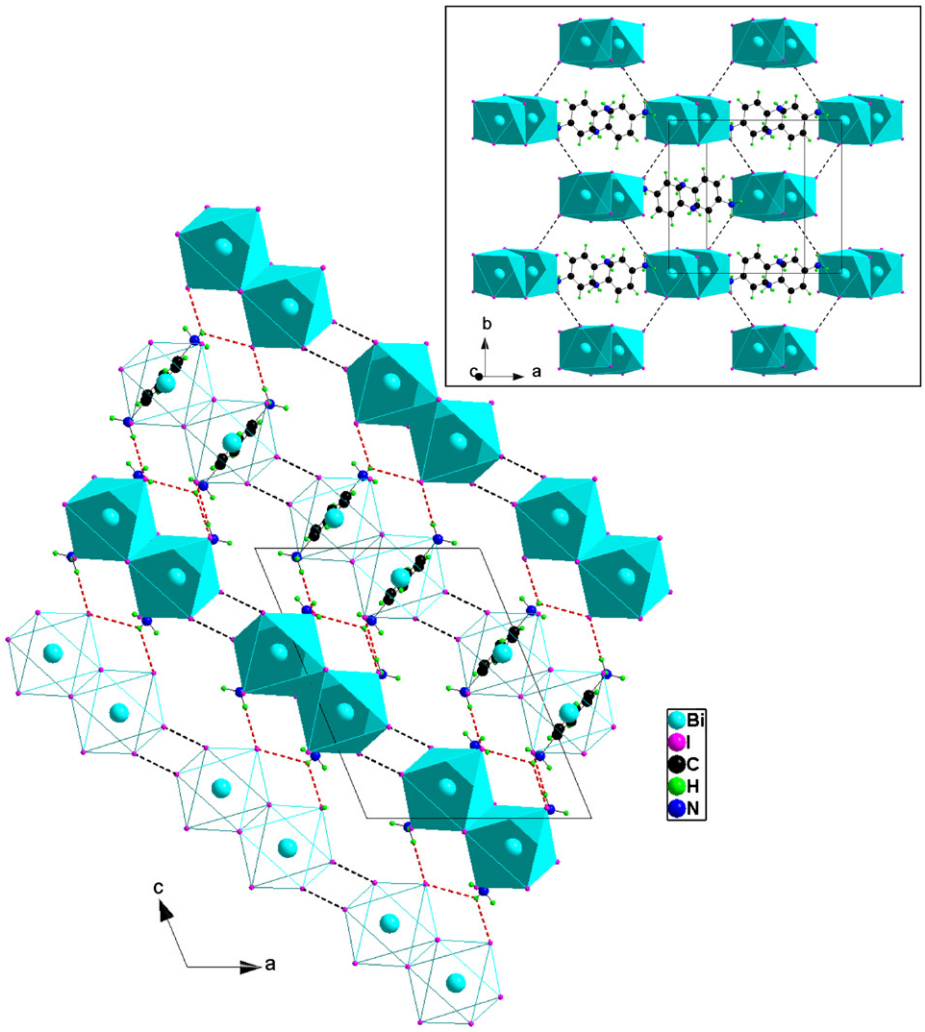

Fig. 3. The layered structure of β-$[C_6H_4(NH_3)_2]_2Bi_2I_{10}$ built up from organic layers separated by the inorganic sheets of $[Bi_2I_{10}]^{4-}$ units described as edge-sharing octahedral (inset shows an electrostatic interactions sheet composed of $[Bi_2I_{10}]^{4-}$ anions with I···I interactions (dashed lines indicate electrostatic interactions)).

Table 3
Hydrogen bonds for α-$[C_6H_4(NH_3)_2]_2Bi_2I_{10}$ and β-$[C_6H_4(NH_3)_2]_2Bi_2I_{10}$.

D–H···A	d(D–H)	d(H···A)	d(D···A)	<(DHA)
α-[C₆H₄(NH₃)₂]₂Bi₂I₁₀				
N1–H11···I1	0.89	3.01	4.080(5)	179.22
N1–H13···I2^{ii}	0.89	2.72	3.417(3)	131.84
N1–H13···I1^{ii}	0.89	3.08	3.703(3)	127.52
N2–H21···I3^{iii}	0.89	3.02	3.949(3)	169.83
N2–H23···I5^{IVi}	0.89	2.74	3.621(6)	156.19
N2–H23···I2^{IVi}	0.89	3.21	3.703(2)	115.67
N2–H22···I4^{Vi}	0.89	2.84	3.512(3)	129.8
N2–H22···I3^{Vi}	0.89	3.09	3.832(3)	136.67
β-[C₆H₄(NH₃)₂]₂Bi₂I₁₀				
N2–H21···I2^{VIi}	0.89	3.06	3.700(2)	133.78
N2–H21···I4^{VIIi}	0.89	3.12	3.837(3)	132.94
N1–H11···I4^{VIIIi}	0.89	3.12	3.667(3)	121.45

ii: x, $-y+1/2$, $z-1/2$, iii: x, y, $z-1$, IVi: $-x$, $-y$, $-z+1$, Vi: x, $-y-1/2$, $z-1/2$, VIi: $x-1/2$, $-y+3/2$, $z-1/2$, VIIi: $-x+1/2$, $y+1/2$, $-z+1/2$, VIIIi: $x+1/2$, $-y+3/2$, $z+1/2$.

type at $-28/-26$ °C (cooling–heating). The phase transition is accompanied by a significant enthalpy transition (ΔH), which equals 1.6 J/g. The temperature hysteresis extrapolated to zero scanning rate for transition was found to be 2 °C.

TG analysis shows that the α-$[C_6H_4(NH_3)_2]_2Bi_2I_{10}$ is stable up to 180 °C and the crystals begin to decompose above *ca* 187 °C. Thermogravimetric experiments confirm the absence of the water molecules of crystallization in the present compound.

3.5. Thermochromism

Interestingly, α-$[C_6H_4(NH_3)_2]_2Bi_2I_{10}$ is a thermochromic material; that is, it changes color as a function of temperature, as can be seen in Table 1. The colors of single crystals of α and β phases taken at different temperatures prior to X-ray data collection illustrate the thermochromic behavior of the compound. On lowering the temperature, the compound with discrete iodobismuthate anions exhibits hypsochromic shift, the color changes from dark-red at 20 °C to orange at -123 °C.

Thermochromic behavior in halobismuthates is known and thought to be due to shifts in the band edge caused by the lattice contraction during cooling. We have observed similar behavior in iodobismuthates [29], where, in fact, BiI_3 itself is thermochromic.

3.6. Optical study

Bismuth-iodide-based hybrids are interesting thanks to the potentially semiconducting character of the inorganic framework.

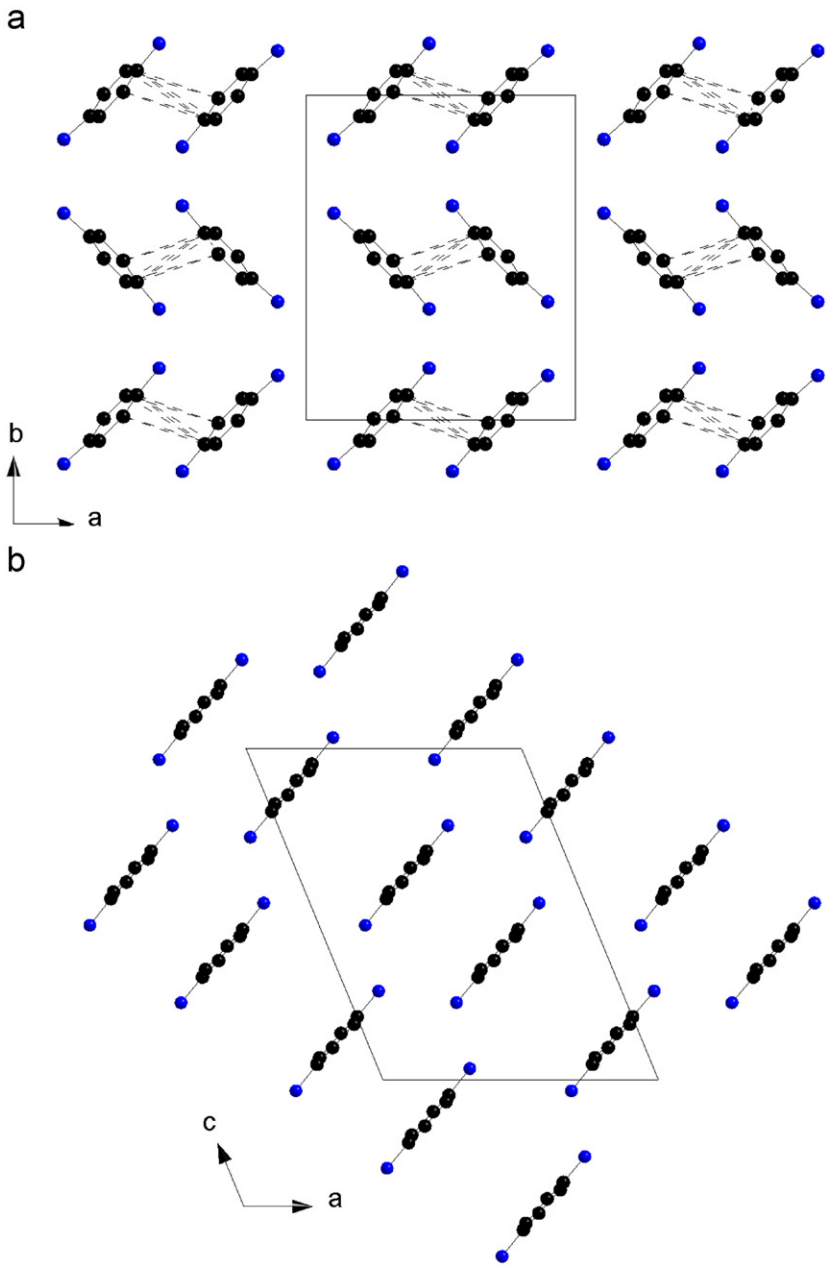

Fig. 4. A View of the layer of cations in the structures of α-$[C_6H_4(NH_3)_2]_2Bi_2I_{10}$ (a) showing the strong π interactions of the *p*-phenylenediammonium. In (b), a similar view for the layer of *p*-phenylenediammonium molecules in crystalline β-$[C_6H_4(NH_3)_2]_2Bi_2I_{10}$ is shown for comparison.

Their optical spectra analysis was performed by analogy with previous studies on organic–inorganic materials containing iodide anions of Bi(III). In fact, previous studies reported in the literature on $(H_2DAH)BiI_5$ [13-c], $(AESBT)_3Bi_2I_9$ [30], $(CH_3NH_3)_3Bi_2I_9$ [31], $[C_6H_4(NH_3)_2]_2Bi_2I_{10}\cdot 4H_2O$ [23] and $[(CH_3)_2NH_2]_3BiI_6$ [32] have shown that the α-$[C_6H_4(NH_3)_2]_2Bi_2I_{10}$ is apparently the third compound containing photoluminescence properties. Hrizi et al. [23], for example, have examined the optical properties of $[C_6H_4(NH_3)_2]_2Bi_2I_{10}\cdot 4H_2O$, which structurally consist of edge-sharing bioctahedral $Bi_2I_{10}^{4-}$ anions (0-D). An absorption band observed at 2.4 eV is assigned to the excitons formed in the inorganic part, and a strong emission band at the energy 2.13 eV is attributed to the excitons confined within the bioctahedra $Bi_2I_{10}^{4-}$. In $(H_2DAH)BiI_5$ [13-c], with its extended BiI_5^{2-} chains (1-D), the exciton peak red-shifts to 2.24 eV, while in the (0-D) $(CH_3NH_3)_3Bi_2I_9$ structure, the direct exciton transition occurs at approximately 2.51 eV [31]. Some energy absorption, photoluminescence and band gaps of these materials are summarized in Table 4.

In the present work, we considered the visible–UV absorption spectrum of the α-$[C_6H_4(NH_3)_2]_2Bi_2I_{10}$ film measured at room temperature (as seen in Fig. 6). Two absorption bands are clearly observed at 2.47 and 3.01 eV. The former has been allotted to an excitonic level formed in the inorganic bioctahedra $Bi_2I_{10}^{4-}$ [31]. The latter is due to electronic transition from the highest occupied molecular orbital (HOMO) to the lowest unoccupied molecular orbital (LUMO). It is generally accepted that the difference (ΔE) between the exciton absorption peak (E_{ex}) and the band gap energy (E_g), $\Delta E = E_g - E_{ex}$, corresponds to the exciton binding energy (E_{BE}). If this relation holds, the exciton binding energy is estimated to be 540 meV and results from both the dielectric and the zero-dimensional quantum confinement effects [23,32]. Fig. 6 shows the room-temperature photoluminescence spectrum for

the bismuth(III) iodide with *p*-phenylenediammonium cation. Regarding α-$[C_6H_4(NH_3)_2]_2Bi_2I_{10}$, the luminescence spectrum was recorded under the excitation of 488 nm. Actually, it shows two luminescence bands that could be observed even with the naked eye at room temperature; a broad one with a maximum at 2.05 eV and a weak one with a maximum at 1.9 eV. These emission peaks may be attributed to the recombination of two types of excitons associated with two different Bi–I bonds. In fact the X-ray diffraction study reveals the existence of non-equivalent asymmetric $Bi_2I_{10}^{4-}$ bioctahedra with a Bi–$I(1)_{bridge}$ bond length of 3.182 and 3.382 Å, respectively. The Stokes shift between absorption at 2.47 eV and emission at 2.05 eV is rather large (420 meV). The luminescence emanates from electronic transitions within the iodobismuthate inorganic part $Bi_2I_{10}^{4-}$. In the bismuth(III) iodide based hybrids, the lowest exciton state arises from the excitations between the valence band consisting of a mixture of Bi(6*s*) and I(5*p*) states, and the conduction band derived primarily from Bi(6*p*) states [23,29,33], and is zero-dimensionally confined in the $Bi_2I_{10}^{4-}$ semiconductor bioctahedra.

It is interesting to compare the absorption, band gaps and luminescence properties of the title compound with those of homologous compounds (as seen in Table 4). It can be clearly seen that the excitonic absorption peaks of zero-dimensional face- and edge-sharing bioctahedrons (2.49 [30], 2.51 [31], 2.4 [23] and 2.47 eV) occur at higher energies than those of the corresponding one-dimensional infinite chains (2.24 eV [13-c]). Besides, the peak of zero-dimensional isolated octahedron (2.6 eV [32]) takes place at a higher energy than those of the corresponding zero-dimensional face- and edge-sharing bioctahedrons. It can also be noted that the band gap energies and PL excitonic peaks exhibit similar behavior to that of excitonic absorption peaks. Such increase in energies is related to the decrease in the structure dimensionality and the anion size, which is comparable to that observed in conventional semiconducting quantum dots and clearly illustrates the quantum confinement effect.

On the other hand, a recent study carried out by Mitzi [13-d] has shown that the shorter *I*···*I* contacts are important structural factors influencing the electronic structure of such hybrids containing lower-dimensional inorganic frameworks. In α-$[C_6H_4(NH_3)_2]_2Bi_2I_{10}$, close interactions (4.069(7)–4.228(2) Å) between iodides on adjacent $[Bi_2I_{10}]^{4-}$ anions within a sheet are confirmed. These inter-iodide distances correspond to approximately twice the ionic radius of an iodide ion, indicating that the binuclear anions were in close contact within the inorganic sheets. It is to be noted that the interactions between inorganic frameworks are essential to the establishment of the electronic and optical properties of the organic–inorganic hybrids and may influence both the underlying electronic structures and the excitons confinement degree within the material.

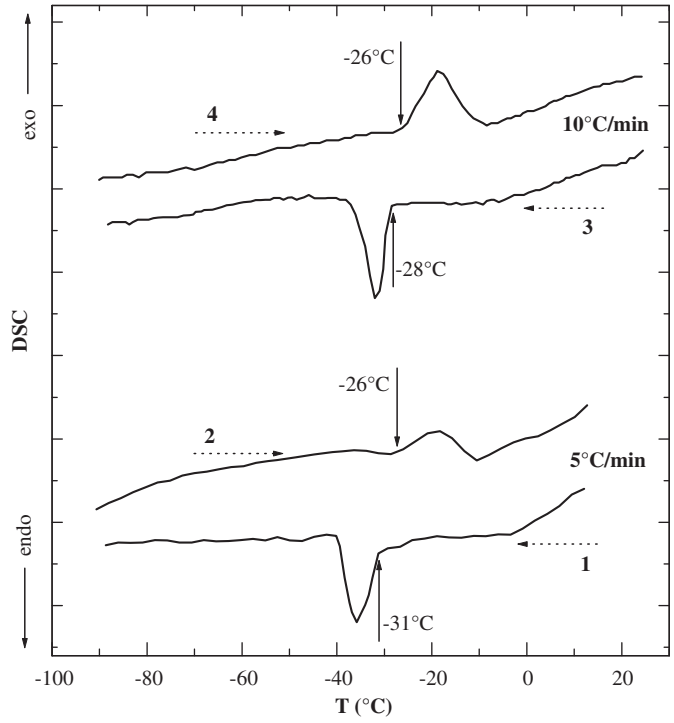

Fig. 5. DSC runs for α-$[C_6H_4(NH_3)_2]_2Bi_2I_{10}$ at the rate of 5 and 10 °C/min upon cooling and heating.

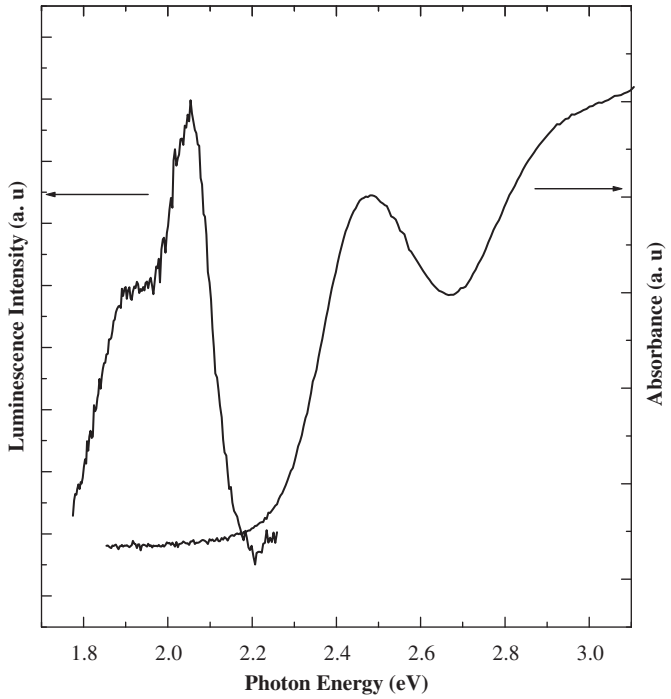

Fig. 6. Room temperature optical absorption and photoluminescence (λ_{ex}=488 nm) spectra of α-$[C_6H_4(NH_3)_2]_2Bi_2I_{10}$.

Table 4
Absorption, photoluminescence and band gaps energy of some homologous compounds reported in the literature.

Compounds	Absorption (eV)	PL (eV)	Band gap (eV)	References
$(H_2DAH)BiI_5$ (1-D) infinite chains	2.24	–	2.48	[13-c]
$(AESBT)_3Bi_2I_9$ (0-D) face-sharing bioctahedra	2.49	–	–	[30]
$(CH_3NH_3)_3Bi_2I_9$ (0-D) face-sharing bioctahedra	2.51	–	2.9	[31]
$[C_6H_4(NH_3)_2]_2Bi_2I_{10}\cdot 4H_2O$ (0-D) edge-sharing bioctahedra	2.4	2.13	2.84	[23]
α-$[C_6H_4(NH_3)_2]_2Bi_2I_{10}$ (0-D) edge-sharing bioctahedra	2.47	1.9/2.05	3.01	Present work
$[(CH_3)_2NH_2]_3BiI_6$ (0-D) isolated octahedron	2.6	2.16	3.04	[32]

4. Conclusion

The present paper has shown that the new organic–inorganic hybrid based on *p*-phenylenediammonium dications and discrete (0-D) iodobismuthate anions, synthesized by slow evaporation, undergoes a reversible structural phase transition at low temperature. This is due to hydrogen bonds and interatomic distances (Bi–I, I···I and π–π) changes within the inorganic sheets and organic layers in the crystal. The crystallographic studies has illustrated that the α-$[C_6H_4(NH_3)_2]_2Bi_2I_{10}$ crystallizes in the centrosymmetric space group $P2_1/c$ at room temperature. Its crystal structure is built from dimeric $[Bi_2I_{10}]^{4-}$ entities with the geometry of two octahedral sharing one edge in the presence of *p*-phenylenediammonium cations. Concerning the DSC experiment, it reveals that it undergoes a reversible phase transition at $-28/-26$ °C accompanied by the modifications of the space group and the unit cell parameters. As for the X-ray examination of this hybrid material at -123 °C, it demonstrates that it crystallizes in the centrosymmetric space group $P2_1/n$. α-$[C_6H_4(NH_3)_2]_2Bi_2I_{10}$ is thermochromic compound as their color change from dark-red at 20 °C to orange at -123 °C. Moreover, after the investigation of the optical properties by optical absorption and photoluminescence measurements, we found red photoluminescence emissions at room temperature assigned to the radiative recombinations of excitons within the bioctahedrons $Bi_2I_{10}^{4-}$.

Supporting Informations

Listings of atomic coordinates and anisotropic motion parameters of α-$[C_6H_4(NH_3)_2]_2Bi_2I_{10}$ and β-$[C_6H_4(NH_3)_2]_2Bi_2I_{10}$, and powder X-ray diffraction, IR and TGA scan for α-$[C_6H_4(NH_3)_2]_2Bi_2I_{10}$.

Appendix A. Supplementary materials

Supplementary data associated with this article can be found in the online version at doi:10.1016/j.jssc.2011.10.004.

References

[1] T. Ishihara, J. Takahashi, T. Goto, Phys. Rev. B 42 (1990) 11 099–11 107.
[2] D.B. Mitzi, S. Wang, C.A. Feild, C.A. Chess, A.M. Guloy, Science 267 (1995) 1473–1476.
[3] P.G. Lacroix, R. Clement, K. Nakatani, J. Zyss, I. Ledoux, Science 263 (1994) 658–660.
[4] J. Takada, H. Awaji, M. Koshioka, A. Nakajima, W.A. Nevin, Appl. Phys. Lett. 61 (1992) 2184–2186.
[5] P. Day, Philos. Trans. R. Soc. London A 314 (1985) 145–158.
[6] Y. Takahashi, R. Obara, K. Nakagawa, M. Nakano, J. Tokita, T. Inabe, Chem. Mater. 19 (2007) 6312–6316.
[7] D.B. Mitzi, C.D. Dimitrakopoulos, J. Rosner, D.R. Meideros, Z. Xu, C. Noyan, Adv. Mater. 14 (2002) 1772–1776.
[8] D.B. Mitzi, K. Chondroudis, C.R. Kagan, IBM J. Res. Dev. 45 (1) (2001) 29–45.
[9] W. Bi, N. Louvain, N. Mercier, J. Luc, I. Rau, F. Kajzar, B. Sahraoui, Adv. Mater. 20 (2008) 1013–1017.
[10] N. Mercier, A.L. Barres, M. Giffard, I. Rau, F. Kajzar, B. Sahraoui, Angew. Chem. 45 (2006) 2100–2103.
[11] A.M. Guloy, Z. Tang, B. Mirana, V.I. Srdanov, Adv. Mater. 13 (2001) 833–837.
[12] (a) G.A. Fisher, N.C. Norman, Adv. Inorg. Chem. 41 (1994) 233–277;
(b) C. Feldmann, J. Solid State Chem. 172 (2003) 53–58;
(c) A.M. Goforth Jr., L. Peterson, M.D. Smith, H.C. zur Loye, J. Solid State Chem. 178 (2005) 3529–3540;
(d) M. Lindsjö, A. Fischer, L. Kloo, Z. Anorg. Allg. Chem. 631 (2005) 1497–1501;
(e) H. Krautscheild, F. Vielsack, J. Chem. Soc. Dalton Trans. 16 (1999) 2731–2735;
(f) W. Bi, N. Louvain, N. Mercier, J. Luc, B. Sahraoui, Cryst. Eng. Commun. 9 (2007) 298–303.
[13] (a) X.H. Zhu, N. Mercier, M. Allain, P. Frere, P. Blanchard, J. Roncali, A. Riou, J. Solid State Chem. 177 (2004) 1067–1071;
(b G.C. Papavassiliou, G.A. Mousdis, C.P. Raptopoulou, A. Terzis, Z. Naturforsch. 54b (1999) 1405–1409;
(c) G.A. Mousdis, G.C. Papavassiliou, A. Terzis, C.P. Raptopoulou, Z. Naturforsch. 53b (1998) 927–931;
(d) D.B. Mitzi, P. Brock, Inorg. Chem. 40 (2001) 2096–2104.
[14] (a) N. Louvain, W. Bi, N. Mercier, J.Y. Buzaré, C. Legein, G. Corbel, Dalton Trans. (2007) 965–970;
(b) S. Chaabouni, S. Kamoun, J. Jaud, J. Chem. Crystallogr. 27 (1997) 727;
(c) M.C. Aragoni, M. Arca, C. Caltagirone, F.A. Devillanova, F. Demartin, A. Garau, F. Isaia, V. Lippolis, Cryst. Eng. Commun. 7 (2005) 544–547;
(d) C. Lode, H. Krautscheild, Z. Anorg. Allg. Chem. 627 (2001) 841–846.
[15] (a) S. Sourisseau, N. Louvain, W. Bi, N. Mercier, D. Rondeau, F. Boucher, J.Y. Buzaré, C. Legein, Chem. Mater. 19 (2007) 600–607;
(b) Z. Xu, D.B. Mitzi, Inorg. Chem. 42 (2003) 6589–6591.
[16] Y. Takeoka, K. Asai, M. Rikukawa, K. Sanui, K. Ishigure, J. Phys. Chem. Solids 61 (2000) 837–845.
[17] D.P. Belotskii, V.B. Timofeev, I.N. Antipov, V.I. Vashchenko, V.A. Bespal'chenko, Russ. J. Phys. Chem. 42 (1968) 740.
[18] G. Fischer, Helv. Phys. Acta 34 (1961) 827–833.
[19] M. Bujak, P. Osadczuk, J. Zaleski, Acta Crystallogr. C55 (1999) 1443–1447.
[20] G.M. Sheldrick, SADABS Bruker AXS Inc., Madison, Wisconsin, USA, 2002.
[21] G.M. Sheldrick, in: G.M. Sheldrick, C. Krüger, R. Goddard (Eds.), SHELXS-86, Crystallographic Computing, vol. 3, Oxford University Press, 1985.
[22] D.J. Watkin, C.K. Prout, J.R. Carruthers, P.W. Betteridge, R.I. Cooper, Crystals, Issue 11, Chemical Crystallography Laboratory, Oxford, UK, 2001.
[23] C. Hrizi, A. Samet, Y. Abid, S. Chaabouni, M. Fliyou, A. Koumina, J. Mol. Struct. 992 (2011) 96–101.
[24] J.P.H. Charmant, N.C. Norman, J. Starbuck, Acta Crystallogr. E58 (2002) m144–m146.
[25] G.A. Bowmaker, P.C. Junk, A.M. Lee, B.W. Skelton, A.H. White, Aust. J. Chem. 51 (1998) 293–309.
[26] R.D. Shannon, Acta Crystallogr. A32 (1976) 751–767.
[27] A. Piecha, V. Kinzhybalo, K. Slepokura, R. Jakubas, J. Solid State Chem. 180 (2007) 265–275.
[28] A. Bondi, J. Phys. Chem. 68 (1964) 441.
[29] M.A. Tershansy, A.M. Goforth, J.R. Gardinier, M.D. Smith, L. Peterson Jr., H.-C. Zur Loye, Solid State Sci. 9 (2007) 410–420.
[30] X.H. Zhu, N. Mercier, P. Frere, P. Blanchard, J. Roncali, M. Allain, C. Pasquier, A. Riou, Inorg. Chem. 42 (2003) 5330–5339.
[31] T. Kawai, S. Shimanuki, Phys. Status Solidi B 177 (1993) K43–K45.
[32] Thesis of Amira Samet, Laboratoire de Physique Appliquée, Université de Sfax, Faculté des sciences de Sfax, BP 1171, 3018 Sfax, Tunisia.
[33] N. Louvain, N. Mercier, F. Boucher, Inorg. Chem. 48 (2009) 879–888.